SLAC-PUB--5419

DE91 008496

PHYSICS AT e^+e^- FACTORIES *

Vera Lüth
Stanford Linear Accelerator Center, Stanford, CA 94309, USA,
and
David B. MacFarlane
McGill University, Montreal, Canada.

ABSTRACT

Feasible designs are well advanced for high-luminosity e^+e^- storage rings which produce $B^0\overline{B}^0$ pairs either at rest or, in what appears to be a more promising option, boosted in the detector frame. Facilities which could provide samples of $30 - 100$ fb^{-1} per year on the $\Upsilon(4S)$ will be proposed in early 1991. Here we examine the principal physics goal of such B Factories, namely CP violation in the b system. Methods in a variety of channels, estimated event samples, and detector requirements are all considered. We conclude that the physics argument for an e^+e^- B Factory is well documented, and compelling.

I. INTRODUCTION

Since the Snowmass study of 1988, the planning, design, and simulation of experiments at high-luminosity e^+e^- storage rings, operating near threshold for $b\bar{b}$ production, have received considerable attention worldwide. There have been numerous workshops sponsored by CERN/PSI [2, 3], Cornell [4], DESY [5], KEK [6], Novisibirsk and SLAC [7, 8] devoted to the subject. Therefore, we have used the occasion of this meeting to critically review the extensive literature which has developed, rather than break much new ground ourselves. This document encompasses a summary of the current ideas for B Factories, in terms of capabilities for b physics. Details may be found in the primary sources referred to below. Participants and contributors are listed in the references [1]. Presentations during the session on ϕ Factories are discussed separately in these proceedings.

Given the limited time and resources at our disposal, we restricted most of our efforts to the physics of CP violation in B decays. Clearly, this is the central theme, and the motivating force behind B Factory proposals. However, in so doing we have ignored another of the great strengths of the e^+e^- Factory approach, namely the multitude of critical measurements in heavy flavour physics which will be performed at these facilities as they ramp up to design luminosities [9]. An essential element of tests of the CKM formulation will be precise determinations of the $b \to c$ and $b \to u$ couplings. Such measurements are likely to require high-statistics studies of exclusive semileptonic or hadronic B decays, and thus the luminosity of a B Factory. A rich program of charm, $\tau^{\pm}$, and two-photon physics will certainly yield important new results.

Presentations and discussions of CP asymmetry due to B^0-$\overline{B}^0$ mixing, or due to interference of competing decay diagrams (so-called "self-tagging" modes), were made. Over the course of the past year, largely in conjunction with the SLAC Detector Workshop [8], mixing induced CP violation has been shown to encompass a large range of experimentally accessible channels, including final states which are CP pure, CP mixtures or even non-CP eigenstates. These can be viewed as either reducing the luminosity estimates required for discovery of CP violation, or as a valuable diagnostic tool in the event that the Standard Model predictions are incorrect. Highlights of this discussion are presented in Section II.

On the detector side, the two critical improvements beyond the present state-of-the-art represented by CLEO II will be in the vertex area and in particle identification above 1.2 GeV/c. In addition to examining the design issues for vertex reconstruction, we also studied the larger question of track parameter resolution for a combined system of silicon, a possible intermediate gas device, and a main drift chamber. Some information was available on the simulated vertex resolution for both the CP and the tagging B decay with nominal silicon configurations. Options for an improved particle identification capability were examined, and the possible impact of the introduction of significant material in front of the electromagnetic

*Work supported by U.S. Department of Energy, Division of High Energy Physics, Contract DE-AC03-76SF00515, and NSERC of Canada.

Invited talk presented at the 1990 DPF Summer Study on High Energy Physics: Research Directions for the Decode, Snowmass, CO, June 25–July 13, 1990.

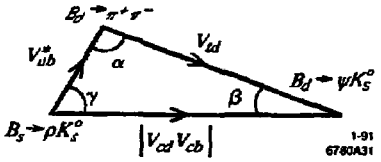

Figure 1: Graphical representation in the complex plane of the relationships between CKM elements imposed by unitarity in three generations.

calorimeter was studied. These issues are addressed in Section III and IV below.

II. MEASURING CP VIOLATION IN B DECAYS

CP violation in B decays is brought about by the interference of two decay amplitudes [10]. A large asymmetry results when the magnitude of these amplitudes is comparable. Such a condition is ensured if both the B^0 and the $\overline{B}^0$ decay to the same final state f, and interference is produced by B^0-$\overline{B}^0$ mixing. If f is an eigenstate of CP, with eigenvalue η_f, so that:

$$CP \mid f \rangle = \eta_f \mid f \rangle$$

and the decay is dominated by a single amplitude w_f, then:

$$\frac{\overline{w}_f}{w_f} = \eta_f e^{-2i\phi_f}$$

where the phase ϕ_f depends only on CKM elements. Starting with an initially pure $B^0(\overline{B}^0)$ state, the time-evolved decay rates into the CP eigenstate f ($\eta_f = +$) are:

$$\Gamma(B^0_{phys} \to f) \propto e^{-\Gamma t}[1 - \mathrm{Im}\lambda \sin(x\Gamma t)]$$
$$\Gamma(\overline{B}^0_{phys} \to f) \propto e^{-\Gamma t}[1 + \mathrm{Im}\lambda \sin(x\Gamma t)]$$

where the amplitude for CP-violation, $\mathrm{Im}\lambda = -\sin 2\phi$, is determined from the CKM phase, $x = \Delta m/\Gamma$ and Δm is the mass splitting between the two neutral B meson mass eigenstates.

Within the three-generation Standard Model, the allowed ranges for the phase ϕ are constrained by measurements of weak interaction couplings. Unitarity of the CKM matrix implies that

$$V_{ud}V_{ub}^* + V_{cd}V_{cb}^* + V_{td}V_{tb}^* = 0,$$

a relationship which can be represented geometrically by a triangle in the complex plane [11]. The lengths

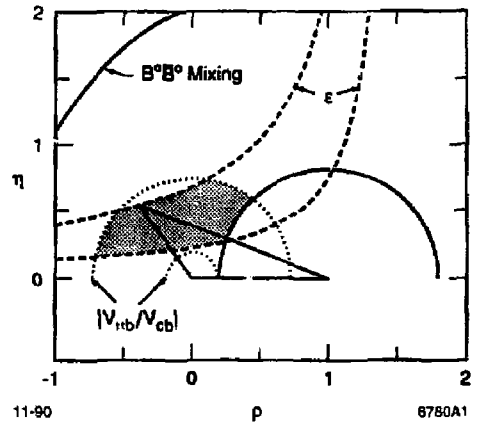

Figure 2: The allowed region (shaded) for the Wolfenstein parameters (ρ, η) given present constraints from $|V_{ub}/V_{cb}|$ (dotted), ϵ_K (dashed) and B^0-$\overline{B}^0$ mixing (solid lines) for top quark mass of 120 GeV/c^2.

of the three sides of this triangle ar defined by B^0-$\overline{B}^0$ mixing (V_{td}), non-charm decays of B mesons (V_{ub}) and a combination of the B lifetime and semileptonic branching ratio (V_{cb}). CP violating asymmetries in neutral B mesons are governed by the interior angles α, β and γ (Figure 1).

Existing measurements of $|V_{cb}|$ and $|V_{ub}/V_{cb}|$ from CLEO [12] and ARGUS [13] provide direct information on the allowed values for CKM parameters; loop processes responsible for CP violation in K^0 decays (ϵ) and B^0-$\overline{B}^0$ mixing (x_d) lead to indirect limitations. A recent analysis of the implications of these data for the unitarity triangle has been made by Dib *et al.* [14]. Their results are expressed in terms of the Wolfenstein [15] variables (ρ, η) and the top quark mass. A representative example of the allowed region is shown in Figure 2, for a top quark mass of 120 GeV/c^2. In this plot the unitarity triangle has a baseline extending from $(\rho, \eta) = (0, 0)$ to $(1, 0)$. The second and third sides of the triangle terminate at any point (ρ, η) in the shaded region, resulting in a range of possible values for the interior angles α, β and γ. Thus, the three angles can assume any value indicated in Figure 3 as a function of the top quark mass. It is noteworthy that, although 90° is not excluded for α or γ (and thus zero asymmetry), the angle β is restricted to lie between 2° and 47°.

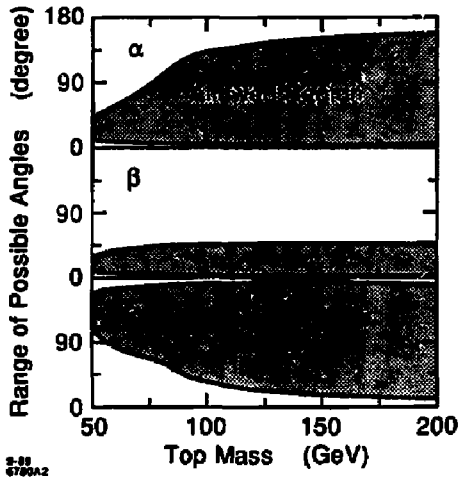

Figure 3: Projections of allowed regions for the three CP angles, as a function of top quark mass.

Strong and electromagnetic processes always produce b quarks in pairs. A measurement of the asymmetry between B^0 and $\overline{B}^0$ decays to a common final state f requires that one of the pair be tagged, while the decay rate of the second is determined. Previous Snowmass studies [16] have examined the relative merits of the existing options for obtaining large samples of b quarks. Here, we concentrate on high-luminosity e^+e^- collisions near $b\overline{b}$ threshold.

The process $\Upsilon(4S) \to B\overline{B}$ has historically proven to be a favourable means of studying b quarks, both because of the production rate and the relatively small background. However, one essential feature for the extraction of CP asymmetries on the $\Upsilon(4S)$ is the prepared nature of the initial-state wave function. It has been shown that for such a $L = 1$, CP-odd pair of B mesons, the tagged asymmetries depend on the time difference $\Delta t = t_1 - t_2$ between the two decays:

$$\Gamma(B^0_{phys} \to f) \propto e^{-\Gamma\Delta t}[1 - \mathrm{Im}\lambda \sin(x\Gamma\Delta t)]$$
$$\Gamma(\overline{B}^0_{phys} \to f) \propto e^{-\Gamma\Delta t}[1 + \mathrm{Im}\lambda \sin(x\Gamma\Delta t)]$$

For a $\Upsilon(4S)$ that is stationary in the detector frame, only a time-integrated measurement is possible, resulting in zero asymmetry. This difficulty can be overcome in two possible ways, both of which have been carefully examined over the past two years:

1. Asymmetric energy e^+e^- collisions, producing a boosted $\Upsilon(4S)$ in the laboratory frame [17].
2. Symmetric energy e^+e^- collisions above the threshold for $B\overline{B}^*$ production.

In the asymmetric option, the $B^0\overline{B}^0$ pair travels along the direction of the high-energy beam, due to the small momentum of the B meson in the $\Upsilon(4S)$ centre-of-mass. The long b lifetime results in a measurable average flight path for the B mesons. The spatial separation of the two decay points along the beam line is then proportional to the time difference between the decays,

$$\Delta t \simeq \Delta z/\beta\gamma c.$$

At least two methods [18] can be applied to recover a finite asymmetry. For example, the events can be divided into four classes, depending on the time-order of the tagging and CP channel decays:

$$\left.\begin{array}{ll} n_1: & B_{tag} = B^0 \\ \overline{n}_1: & B_{tag} = \overline{B}^0 \end{array}\right\} t_{\mathrm{CP}} < t_{tag}$$
$$\left.\begin{array}{ll} n_2: & B_{tag} = B^0 \\ \overline{n}_2: & B_{tag} = \overline{B}^0 \end{array}\right\} t_{\mathrm{CP}} > t_{tag}$$

Interference in the partial rates for the four classes is illustrated conceptually in Figure 4. Taking appropriate sums and differences of the observed numbers of events, a non-zero asymmetry can be measured:

$$A_{\mathrm{CP}} = \frac{(n_1 - \overline{n}_1) - (n_2 - \overline{n}_2)}{n_1 + \overline{n}_1 + n_2 + \overline{n}_2} = -d_0 \sin 2\phi,$$

with an effective dilution factor $d_0 = x_d/(1 + x_d^2) \simeq 0.47$. A more sensitive technique is to fit the distribution of vertex separation Δz, after division into classes with positive $(n_1 + \overline{n}_2)$ and negative $(\overline{n}_1 + n_2)$ interference. The dilution factor then becomes $d_0 \simeq 0.58$ [19] (Figure 5).

Above the threshold for $B\overline{B}^*$ production, the decay to $B\overline{B}\gamma$ leads to a $B^0\overline{B}^0$ pair in an $L = 0$, CP even state. The tagged partial widths in this case depend on the sum, $t_1 + t_2$, of the decay times:

$$\Gamma(B^0_{phys} \to f) \propto e^{-\Gamma(t_1+t_2)}[1 - \mathrm{Im}\lambda \sin x\Gamma(t_1 + t_2)]$$
$$\Gamma(\overline{B}^0_{phys} \to f) \propto e^{-\Gamma(t_1+t_2)}[1 + \mathrm{Im}\lambda \sin x\Gamma(t_1 + t_2)].$$

The time-integrated asymmetries are non-zero, with a dilution factor $d_0 = 2x_d/(1 + x_d)^2$ of about 63%.

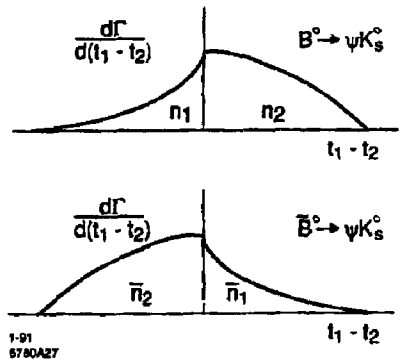

Figure 4: Separation of events into classes with positive and negative CP interference, depending on time order of tag and CP decays.

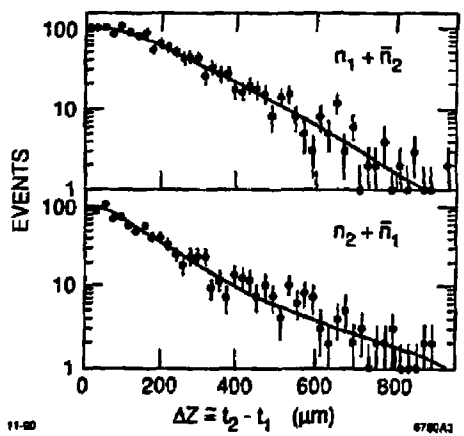

Figure 5: Example of a fit to the distribution of longitudinal vertex separation Δz between tag and CP channel. The statistics corresponds to 2300 tagged decays.

Clearly this approach requires that the experiment be run at centre-of-mass energies above the $\Upsilon(4S)$, with a corresponding reduction in cross section. The observed cross section above the resonance is approximately 0.3 nb above the continuum level [20]. Attempts to directly measure the $B\overline{B}$ cross section in this region are underway at CESR.

The luminosity required to achieve an asymmetry measurement of a specified significance $s = A_{CP}/\sigma_A$ is given by [21]:

$$\int \mathcal{L}dt = \frac{s^2}{2\sigma_{b\bar{b}} f_0 \epsilon_R B R_{CP} \epsilon_{tag} A_{CP}^2} \frac{1 + S/B}{S/B}$$

where

A_{CP}	=	$(1-2w)d_0 \sin 2\phi$
$\sigma_{b\bar{b}}$	=	Cross section for $b\bar{b}$
f_0	=	$B^0\overline{B}^0$ fraction
BR_{CP}	=	Branching ratio for CP mode
ϵ_R	=	Reconstruction efficiency
ϵ_{tag}	=	Tagging efficiency
w	=	Fraction of wrong-sign tags
d_0	=	Dilution factor
S/B	=	Signal-to-Background ratio

Several Monte Carlo studies have been made to estimate efficiencies, vertex resolution, tagging efficiencies and purities, and signal-to-background ratios in a variety of channels [7, 8, 22]. These are based on reasonable assumptions about the detector configuration, along the lines discussed below in Sections III and IV. In some cases, for example kaon tagging efficiency, we have tried to make a rational interpolation of the available estimates. Results for $B^0 \to J/\psi K_S^0$ and $\pi^+\pi^-$, the primary examples of CP eigenstates, are summarized in Tables 1 and 2 respectively. Per unit of delivered luminosity, the symmetric collider appears to be at least a factor of three, and more likely an order of magnitude, less sensitive than the asymmetric option depending on the channel considered. Small advantages in acceptance and the more favourable value for the dilution factor do not overcome the large cross section penalty. Furthermore, better background suppression is generally available at the asymmetric collider, due to vertex constraints. Implicit in this statement are many assumptions about the detector, particularly the vertex region, which will be discussed below.

Table 1: Comparison of sensitivity in the channel $B^0 \to J/\psi K^0_S$ for asymmetric versus symmetric energy collisions.

	Asymmetric $\Upsilon(4S)$	Symmetric $\Upsilon(4S)^+$
$\sigma_{b\bar{b}}$ [nb]	1.2	0.13-0.3
f_0	0.5	0.45
ϵ_R	0.58	0.65
ϵ_{top}	0.45	0.50
w	0.07	0.07
d_0	0.58	0.63
BR_{CP}	3.7×10^{-4}	3.7×10^{-4}
$\mathcal{L}/\mathcal{L}(Asym)$	1.0	3.0-6.9

Table 2: Comparison of sensitivity in the channel $B^0 \to \pi^+\pi^-$ for asymmetric versus symmetric energy collisions.

	Asymmetric $\Upsilon(4S)$	Symmetric $\Upsilon(4S)^+$
$\sigma_{b\bar{b}}$ [nb]	1.2	0.13-0.3
f_0	0.5	0.45
$\epsilon_R \times \epsilon_{top}$	0.215	0.215
S/B	22.5	4.8
w	0.07	0.07
d_0	0.58	0.63
BR_{CP}	2×10^{-5}	2×10^{-5}
$\mathcal{L}/\mathcal{L}(Asym)$	1.0	6.9-16.0

III. ALTERNATIVE CHANNELS

In parallel with the tremendous advances in designing high-luminosity facilities for b physics, a fruitful and systematic examination of other possible CP violating channels has been made. It has been shown that the requirement that the final state be a CP eigenstate can be relaxed, without sacrificing the predictability which is a key component in using B decays for precision tests of the Standard Model. A summary of possible extensions is provided in Table 3 below [23]. Specific examples from several of the new categories are examined in the following sections.

A. Analysis of States with Mixed CP Eigenstates

Dilution of Asymmetry

Many decay modes of the B^0 involving three particles, or two particles with spin, are mixtures of different CP eigenstates. Therefore the measured CP asymmetry will depend on the ratio of CP-even and CP-odd states. The decay rate of a state that evolved from an initially pure $B^0(\overline{B}^0)$ to the final state $f(\overline{f})$ can be written in the form

$$\Gamma(B^0_{\rm phys} \to f) = \Gamma_+(1+a) + \Gamma_-(1-a),$$

$$\Gamma(\overline{B}^0_{\rm phys} \to \overline{f}) = \Gamma_+(1-a) + \Gamma_-(1+a).$$

The CP-even and CP-odd rates are denoted by the widths Γ_+ and Γ_-, respectively. The rates are time dependent and Γ_+ and Γ_- contain a factor $e^{-\Gamma t}$, where Γ is the average width of the B^0 mass eigenstates.

The measured asymmetry is

$$\frac{\Gamma(B^0_{\rm phys} \to f) - \Gamma(\overline{B}^0_{\rm phys} \to \overline{f})}{\Gamma(B^0_{\rm phys} \to f) + \Gamma(\overline{B}^0_{\rm phys} \to \overline{f})} = a\,\frac{\Gamma_+ - \Gamma_-}{\Gamma_+ + \Gamma_-}.$$

with $a = -{\rm Im}\lambda \sin(x\Gamma t)$. The last factor gives the dilution that occurs if the final state f is a mixture of CP-even and CP-odd parities. If an analysis of angular distributions can be made for each time-bin separately (since the asymmetry is different at different times) this dilution can be avoided, regardless of the Γ_+/Γ_- ratio.

Several methods have been discussed which can be used to reconstruct CP eigenstates from a superposition of helicity states. The first method analyzes decays in terms of a quantity called transversity, which characterizes the spin projections of a three body state in the direction transverse to the momentum plane

Table 3: B decay channels available for mixing-induced CP violation searches.

	Class	Examples
1.	$B^0 \to f$, $\overline{B}^0 \to f$ where f = CP Eigenstate	$J/\psi K^0_S$ $\pi^+\pi^-$ D^+D^-
2.	$f = (A)_{CP}(B)_{CP}$ or $A\overline{A}$ where A, B have spin	$J/\psi\rho^0$ $D^{*+}D^{*-}$
3.	$f = (A)_{CP}B$ where $B \to (C)_{CP}$	$J/\psi K^{*0}$, $K^{*0} \to K^0_S\pi^0$ $\overline{D}^0\pi^0$, $\overline{D}^0 \to \pi^+\pi^-$
4.	f = 3-body state (a) CP Eigenstate (b) Mixture of CP States	 $\eta_C K^0_S\pi^0$ $J/\psi K^0_S\pi^0$
5.	$f = A_1\overline{A}_2$ where $A_1\overline{A}_2 = (q_x\overline{q}_y)(\overline{q}_x q_y)$ (CP self-conjugate set of quarks)	$d\bar{d}c\bar{c} \equiv D^{*+}D^-$ $d\bar{d}s\bar{s} \equiv K^{*0}\overline{K}^0$ $d\bar{d}u\bar{u} \equiv \rho^\pm\pi^\mp$, $a_1^\pm\pi^\mp$

[24]. This approach has the advantage that the analysis can be performed with the combined sample of resonant and non-resonant contributions to a given final state, whereas the more detailed angular analysis requires reconstruction of a specific two-body parent system for the three-body state.

The second method uses a more complete angular analysis and forms all possible independent angular moments of the data. These moments project out certain linear combinations of helicity amplitudes which can be formed into CP eigenstates [25]. This permits the study of additional channels not amenable to the transversity treatment. Like the transversity moment analysis, this method has the advantage that it allows asymmetries to be extracted without *a priori* knowledge of the relative strengths of the different helicity contributions. In both cases this can be done by combining results from B^0 and $\overline{B}^0$ decays.

Two other methods are based on maximum-likelihood fits to the angular distributions of the CP-violating decays and to a set of isospin-related decay channels that are not affected by CP violation [26]. This can be done by using either the transversity polar angle distributions alone or the complete angular distributions. For a transversity analysis of this type one needs to know the relative strengths of the contributions for each possible absolute value of the transversity. In most cases this can be determined from isospin-related channels [27]. For the complete angular analysis the full set of helicity amplitudes and their relative strong-interaction phases need to be determined. In the limit of very large statistics, this method will provide the most accurate measure of the asymmetry.

Transversity Analysis

In the following, the concept of transversity will be introduced as an analyzer for CP parities in three body decays of the B^0, a spinless neutral particle [24]. The three final-state momenta define a plane and are invariant under reflections in the plane. Such a reflection can be written as the product of a space inversion P and a 180° rotation about an axis normal to the plane, which we select to be the z axis:

$$R_{xy} \equiv P e^{i\pi J_z} = P_{int} \cdot e^{i\pi\tau},$$

where P_{int} denotes the total intrinsic parity of the three particle system, J_z is the projection of the total angular momentum of the three particle state on the z axis and τ denotes the sum of the transversities of the three particles, i.e. the projection of the total spin angular momentum of the state on the z axis. The equality follows because all three momenta in the centre-of-mass system remain invariant under R_{xy} and therefore only the internal degrees of freedom contribute.

Since the initial state has spin zero, the final state must also have spin zero and be invariant under rotations in the centre-of-mass system. For any $J = 0$ state

$$
\begin{aligned}
R_{xy} \mid J=0\rangle &\approx P e^{i\pi J_x} \mid J=0\rangle \\
&\approx P_{int} \cdot e^{i\pi\tau} \mid J=0\rangle \\
&\approx P \mid J=0\rangle
\end{aligned}
$$

and it follows that

$$
\begin{aligned}
CR_{xy} \mid J=0\rangle &\equiv CP e^{i\pi J_x} \mid J=0\rangle \\
&= (CP)_{int} \cdot e^{i\pi\tau} \mid J=0\rangle \\
&= CP \mid J=0\rangle .
\end{aligned}
$$

Thus in decays such as $B^0 \to J/\psi K^0_S \pi^0$ and $B^0 \to \eta_C K^0_S \pi^0$, where each of the three particles in the final state has a definite intrinsic parity and intrinsic charge conjugation, the CP eigenvalue of the state can be determined by a measurement of the transversity.

For the final state $J/\psi K^0_S \pi^0$ with $(CP)_{int} = -1$, and thus we have $CP \approx -1$ for $\tau = 0$, and $CP = +1$ for $\tau = \pm 1$. The same holds for all radial excitations of the J/ψ. The two CP states can be distinguished by the angular distribution of the lepton pairs from the decay $J/\psi \to \ell^+\ell^-$ relative to the momentum of the J/ψ. In fact, the ARGUS collaboration has shown that inclusive J/ψ from B decays in the two-body momentum interval are strongly polarized. A fit of the form $1+\alpha\cos^2\theta_{\ell+}$ to the distribution of the angle $\theta_{\ell+}$ between the lepton direction and the J/ψ boost direction in the J/ψ rest frame gives $\alpha = -1.17 \pm 0.17$. This means that the state is dominated by $\tau = 0$, i.e. the state is $CP = -1$ [28]. Consequently the dilution of the asymmetry is small, and the sensitivity of the decay $B^0 \to J/\psi K^{*0}$ is expected to be comparable to that for the decay $B^0 \to J/\psi K^0_S$.

For the final state $\eta_C K^0_S \pi^0$, which has $(CP)_{int} = +1$ and $\tau = 0$ for three spinless particles, we find that $CP = +1$ for all possible partial waves in the final state, including the states where the $K\pi$ system forms a K^* resonance. This can be derived by examining the intrinsic P and C and all allowed partial waves. K^0_S is a CP=+1 state, and η_C and π^0 are $CP = -1$ states. There are two relative orbital angular momenta for this three-body system, but they must both be equal in order to couple to the spin zero required by angular momentum conservation. Thus although all values of this orbital angular momentum are allowed, all have even orbital parity and even intrinsic CP.

The final state $D^{*+}D^{*-}$ contains several partial waves and can have $CP = +1$ and $CP = -1$. A transversity measurement can be used to separate the different CP eigenstates. Since the total angular momentum has to be J=0 for the decay of a spinless particle, $L = S$ for the orbital angular momentum, and the CP eigenvalue for this state equals P, the parity eigenvalue. Since the intrinsic parity of the $D^{*+}D\pi$ system is $P = -1$, it follows that the CP eigenvalue for the whole system is $CP = -1$ if $\tau = 0$ for the D^{*+}, and $CP = +1$ for non-zero transversity, $\tau = \pm 1$.

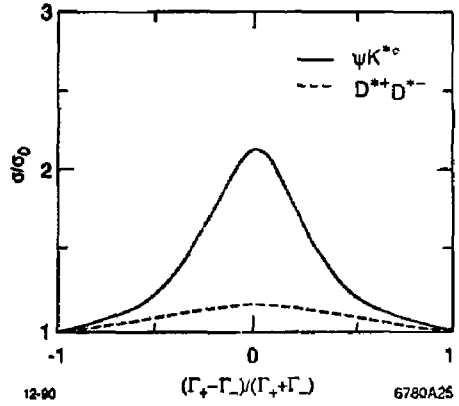

Figure 6: Increase in the uncertainty of the CP violating asymmetry as a function of the CP mixture in the decays $J/\psi K^{*0}$ and $D^{*+}D^{*-}$.

Even though one can use the transversity analysis to measure the mixture of the CP eigenstates in a given decay mode, the error for a mixed sample is always larger than for a pure sample. Figure 6 shows the increase in the error on the CP violating asymmetry as a function of the mixture for two decay modes [29]. The final state $D^{*+}D^{*-}$ is less sensitive to the mixture than the state $J/\psi K^{*0}$, but based on the ARGUS measurement we already know that this decay mode is dominated by the $CP = +1$ state.

B. Final States of CP Self-Conjugate Quarks

CP asymmetries where the final state f is made up of a pair of mesons differing in mass or J^{PC}, but which at the quark level consists of a CP self-conjugate collection of quarks (Class 5), offer an important expansion of the experimentally accessible channels. The general formalism which is used to describe decays to non-CP eigenstates can be found in reference [30]. Examples which have been considered in considerable detail are $B^0 \to \rho^\pm\pi^\mp$ and $a_1^\pm\pi^\mp$. Supposing that

both B^0 and $\overline{B}^0$ can reach a final state f, or its CP conjugate state $\overline{f}$, then:

$$\begin{aligned}
\langle f \mid \overline{B}^0 \rangle &= e^{i\phi_f} e^{i\alpha} M \\
\langle f \mid B^0 \rangle &= e^{-i\phi'_f} e^{i\alpha'} M' \\
\langle \overline{f} \mid B^0 \rangle &= e^{-i\phi_f} e^{i\alpha} M \\
\langle \overline{f} \mid \overline{B}^0 \rangle &= e^{i\phi'_f} e^{i\alpha'} M'
\end{aligned}$$

where $\phi^{(\prime)}$ and $\alpha^{(\prime)}$ are the CKM and strong interaction phases respectively, and the $M^{(\prime)}$ are the magnitudes of the decay amplitudes. Interference via B^0-$\overline{B}^0$ mixing results in tagged decay widths:

$$\begin{aligned}
\Gamma({}^{(}\overline{B}{}^{)0}_{phys} \to f) \propto e^{-\Gamma t}[1 \, {}^{(}\pm{}^{)} \\
\beta \cos x\Gamma t \, {}^{(}\pm{}^{)} \sqrt{1-\beta^2} \sin\phi_1 \sin(x\Gamma t)] \\
\Gamma({}^{(}\overline{B}{}^{)0}_{phys} \to \overline{f}) \propto e^{-\Gamma t}[1 \, {}^{(}\mp{}^{)} \\
\beta \cos x\Gamma t \, {}^{(}\pm{}^{)} \sqrt{1-\beta^2} \sin\phi_2 \sin(x\Gamma t)]
\end{aligned}$$

where $\rho = M_1/M_2$, $\beta = (\rho^2-1)/(\rho^2+1)$, and the angles $\phi_{1(2)} = 2\phi \, {}^{(}\mp{}^{)}(\alpha_1 - \alpha_2)$ depend on the phases introduced by B^0-$\overline{B}^0$ mixing and the weak decay amplitudes: $\phi = 2\phi_{mix} + \phi_f + \phi'_f$. There are four measurements available to determine three unknowns. In particular, the appropriate sums of partial widths:

$$\begin{aligned}
\Gamma({}^{(}\overline{B}{}^{)0} \to f) + \Gamma({}^{(}\overline{B}{}^{)0} \to \overline{f}) \propto e^{-\Gamma t}[1 \, {}^{(}\pm{}^{)} \\
\sqrt{1-\beta^2} \cos(\alpha_1 - \alpha_2) \sin 2\phi \sin x\Gamma t]
\end{aligned}$$

reproduce our previous result for CP eigenstates, with an effective dilution factor $d_0 = \sqrt{1-\beta^2}\cos(\alpha_1 - \alpha_2)$. For experiments on the $\Upsilon(4S)$, the initial state correlation requires a time-ordered measurement, so that t is once more replaced by Δt in this case. It should also be noted that there is a four-fold sign ambiguity in extracting $\sin 2\phi$. It is possible that some solutions are unphysical. Alternatively studies in related channels may resolve the problem.

The size of the asymmetry, and hence the improvement in sensitivity brought by the new channels, depends on the ratio of the decay widths for $B^0 \to f$ versus $B^0 \to \overline{f}$. For the particular examples considered here, factorization leads to reliable predictions for the ratio of branching ratios to $\pi^+\pi^-$ in terms of a_1^-, ρ^- and π^- form factors, since all three originate from the W^- decay. Thus, one expects [30]:

$$\frac{\Gamma(\overline{B}^0 \to \rho^-\pi^+)}{\Gamma(\overline{B}^0 \to \pi^-\pi^+)} = \left|\frac{F_\rho}{F_\pi}\right|^2 \simeq 2$$

Moreover, final-state phases are expected to be small for B decays to two light particles. Neglecting backgrounds and efficiencies, the relative sensitivity can then be expressed as:

$$\frac{\sigma[\sin 2\alpha]_{\rho^\pm\pi^\mp}}{\sigma[\sin 2\alpha]_{\pi^+\pi^-}} \simeq \sqrt{\frac{\rho^2+1}{8\rho^2}}$$

as illustrated in Figure 7. One concludes that for $\rho^2 = \Gamma(\overline{B}^0 \to \rho^+\pi^-)/\Gamma(\overline{B}^0 \to \rho^-\pi^+)$ greater than $1/7$, the new channel is more sensitive to $\sin 2\alpha$ than $\overline{B}^0 \to \pi^+\pi^-$.

A realistic Monte Carlo simulation [30] has been performed, leading to the estimated measurement errors shown in Figure 8 for $\overline{B}^0 \to \rho^\pm\pi^\mp$ and $a_1^\pm\pi^\mp$. For this study, preselection cuts were based on the mass of the B candidate and the energy in the $\Upsilon(4S)$ rest frame, the masses of all intermediate states (a_1, ρ, or π^0), and a quality of the vertex formed from charged particles in the decay. Both leptons and single kaons were used for tagging the second B mesons, with perfect particle identification assumed. The achieved signal-to-background ratios were decidedly worse than those obtained for $\overline{B}^0 \to \pi^+\pi^-$, ranging from 1 for lepton tagged $\rho^\pm\pi^\mp$ to 16 for kaon tagged $a_1^\pm\pi^\mp$. These would be sufficiently large to significantly degrade sensitivity in some cases. However, in a second stage a cut variable ("rarity") was constructed by using coherently the mass and energy constraints, along with an event shape variable, to discriminate against the continuum backgrounds. This produced much more promising results, with some further loss in efficiency (Table 4). The authors conclude that the non-CP channels will turn out to be more sensitive than $\overline{B}^0 \to \pi^+\pi^-$.

C. Summary of CP Phase Measurements

A summary of present estimates for event samples, and corresponding errors on asymmetries, are indicated in Table 5 for both $\sin 2\beta$ and $\sin 2\alpha$ for a typical asymmetric B Factory at a luminosity of 3×10^{33} cm^2 s^{-1}. The addition of new channels extends the range of sensitivity to include most of the allowed region for the two angles α and β.

D. Direct CP Violation

So far, we have considered CP violation in decay modes that are not flavour specific, i.e. final states that are common to B^o and $\overline{B}{}^o$ decays. In these decay modes CP violation is observable as a time dependent asymmetry caused by interference due to B^o–$\overline{B}{}^o$ mixing, i.e. $\Delta B = 2$ transitions. In flavour specific decays of both neutral and charged B mesons, we expect a time-independent asymmetry due to so-called

Table 4: Background-to-signal ratios before and after the coherent suppression cut, the relative efficiency, ϵ^*, and the remaining degradation of sensitivity due to background, s/s_0, separately for lepton and kaon tagged samples of three decay modes.

	$\pi^+\pi^-$		$\rho^\pm\pi^\mp$		$a_1^\pm\pi^\mp$	
	Lepton	Kaon	Lepton	Kaon	Lepton	Kaon
B/S before	1	8	2	16	0.02	0.18
B/S after	0.13	0.42	0.27	0.57	0.01	0.09
ϵ^*	0.93	0.76	0.89	0.62	1	1
s/s_0	10%	40%	20%	60%	0.6%	5%

Table 5: Summary of estimated branching ratios, efficiencies and sensitivities for representative channels which can be used to determine CP asymmetries. The combined error from the three channels would be about ± 0.06 and ± 0.086 for $\sin 2\beta$ and $\sin 2\alpha$, respectively.

Measurements	Mode		
of $\sin 2\beta$	$J/\psi K_S^0$	$J/\psi K^{*0}$	D^+D^-
Final State	$\ell^+\ell^-\pi\pi$	$\ell^+\ell^-\pi^+\pi^-\pi^0$	many
BR_B	7.4×10^{-4}	12.5×10^{-4}	6×10^{-4}
BR_{decay}	7×10^{-2}	1.5×10^{-2}	3.6×10^{-2}
ϵ_R	0.58	0.46	0.30
ϵ_{tag}	0.45	0.45	0.45
N_{obs}	487	144	105
$\sigma[\sin 2\beta]$	0.077	0.14	0.17

Measurements	Mode		
of $\sin 2\alpha$	$\pi^+\pi^-$	$\rho^\pm\pi^\mp$	$a_1^\pm\pi^\mp$
Final State	$\pi^+\pi^-$	$\pi^+\pi^-\pi^0$	$\pi^+\pi^-\pi^+\pi^-$
BR_B	2×10^{-5}	6×10^{-5}	6×10^{-5}
BR_{decay}	1.0	1.0	0.5
ϵ_R	0.45	0.48	0.42
ϵ_{tag}	0.45	0.45	0.45
N_{obs}	142	464	207
$\sigma[\sin 2\alpha]$	0.18	0.12	0.18

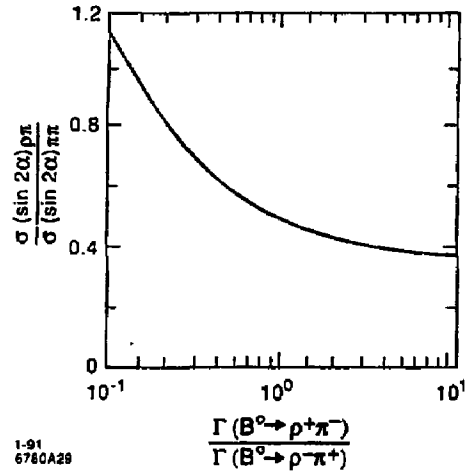

Figure 7: Relative error of the CP asymmetry measurement as a function of the ratio of decay widths for $\overline{B}^0 \to \rho^+\pi^-$ over $\overline{B}^0 \to \rho^-\pi^+$.

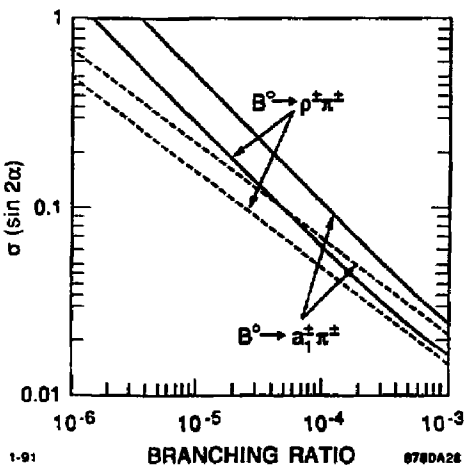

Figure 8: Monte Carlo simulation of sensitivity to $\sin 2\alpha$ for $\overline{B}^0 \to \rho^\pm\pi^\mp$ and $a_1^\pm\pi^\mp$ in a 50 fb^{-1} sample. Solid and dotted lines refer to the resolution that could be achieved with or without background, respectively.

direct CP violation in the decay amplitude itself, i.e. $\Delta B = 1$ transitions. When two different amplitudes contribute to the decay of a B meson to a final state f, the amplitude for the decay can be written as

$$\begin{aligned}\langle f \mid \mathcal{L}(\Delta B = 1) \mid B\rangle &= \langle f \mid \mathcal{L}_1 \mid B\rangle + \langle f \mid \mathcal{L}_2 \mid B\rangle \\ &= g_1 M_1 e^{i\alpha_1} + g_2 M_2 e^{i\alpha_2}.\end{aligned}$$

M_1, M_2 denote the matrix elements for the weak interaction operators $\mathcal{L}_1, \mathcal{L}_2$ with the CKM parameters g_1, g_2 and the strong (or electromagnetic) phase shifts α_1, α_2. The amplitude of the CP conjugate state decay $\overline{B} \to \overline{f}$ then reads:

$$\langle \overline{f} \mid \mathcal{L}(\Delta B = 1) \mid \overline{B}\rangle = g_1^* M_1 e^{i\alpha_1} + g_2^* M_2 e^{i\alpha_2},$$

where the CP invariance of the strong interaction fixes the phase shifts. A difference in rate for the two processes establishes CP violation, and we have

$$\Gamma(B \to f) - \Gamma(\overline{B} \to \overline{f}) \propto \mathrm{Im}\, g_1^* g_2 \sin(\alpha_1 - \alpha_2) M_1 M_2.$$

This rate difference can only be non-zero if two conditions are met simultaneously:

1. the two non-trivial phase shifts $\alpha_1 \neq \alpha_2$ have to be present, and
2. there has to be a relative complex phase between the two weak couplings g_1 and g_2.

It turns out that processes that fulfil these conditions involve at the quark level loop diagrams with a gluon or photon, usually referred to as penguin diagrams. These diagrams generate an absorptive part due to on-mass-shell rescattering of a virtual gluon with four-momentum $q^2 > 4m_q^2$, where m_q refers to the mass of the intermediate quark u or c. At the same time, loops with contributions from different generations of quarks produce complex CKM phases. While there is agreement among theorists that rescattering is bound to occur there are widely differing opinions about the scheme and the reliability of calculations of its effect on the rate and the asymmetry in exclusive decay modes [31] [32] [33]. Figure 9 shows an example for two amplitudes that could lead to direct CP violation in decays such as $B^+ \to K^+\pi^\circ$ or $B^\circ \to K^+\pi^-$. At the workshop, N.G. Deshpande estimated the expected rates and asymmetries for processes involving interference between two amplitudes of comparable size, either a penguin and a CKM suppressed spectator amplitude or two penguin amplitudes. While the relative rates for penguin transition

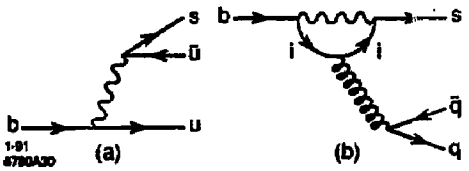

Figure 9: Quark diagrams for the process $b \to s\bar{u}u$.

$b \to d$ to $b \to s$ are suppressed by a factor λ^2, $u\bar{u}$ is expected to be suppressed relative to $c\bar{c}$ by a factor of roughly λ^4. The results are listed in Table 6, they are to be taken as rough order of magnitude estimates. There remain substantial uncertainties in the theoretical assumptions, in particular for calculating exclusive rates, though most theorists expect that some of these processes will lead to significant CP violating effects.

From an experimental point of view, it is very interesting to learn that some of these asymmetries may be sizable, though most of the branching ratios are expected to be small. The decay modes listed represent rather simple final state with relatively good detection efficiencies. Also, the measurement of the asymmetry in these self-tagging modes does not require any vertex detection or tagging of the second B decay. This opens the possibility that such affect may be detectable in hadronic production of B mesons were production rates are very large. However, to produce a convincing effect, the experimenters will have to make sure that the detector has equal sensitivity to the two charge conjugate state, this is somewhat reminiscent of measurements of the CP violating charge asymmetry in semi-leptonic K^0 decays.

IV. MEASUREMENT OF THE TIME DEPENDENT ASYMMETRY

A. Vertex Resolution

The primary physics goal of an asymmetric B factory is the measurement of the time evolution of the B^0-$\overline{B}^0$ asymmetry in decays to CP eigenstates, caused by interference between the mixed and unmixed B mesons. The relevant time is the difference in proper time between the two decays, Δt, which is to a very good approximation proportional to the difference in decay distances. The resolution in measuring this difference in decay lengths Δz should be good enough so as not to significantly degrade the measurement of this asymmetry.

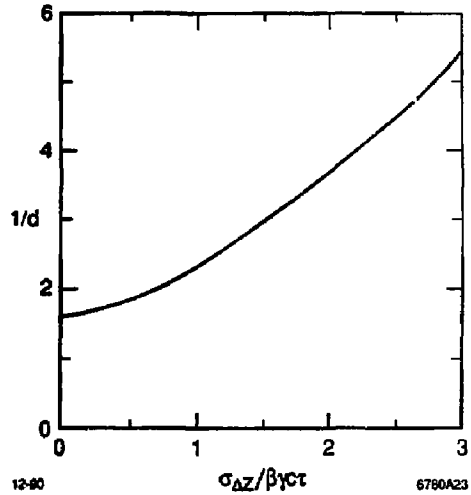

Figure 10: Dilution of the measurement of the CP asymmetry as a function of $\sigma_{\Delta z}$, the resolution in the decay distance of the two B^0 mesons.

A number of studies have been performed to investigate the specifications for the vertex detector resolution, simulating the process $B^0 \to f_1$ and $\overline{B}^0 \to f_2$, where f_1 represents a CP eigenstate, like $J/\psi K^0_S$, and f_2 is a decay that tags the identity of the B meson, like the semi-leptonic decay to $D^+\ell^-\nu$. In the presence of CP violation, the decay rate of a $(\overline{B})^0$ to a CP eigenstate f_1 is

$$R \propto e^{-\Gamma|\Delta t|}[1 \mp \sin 2\phi \ \sin(x\Gamma\Delta t)] \ G_m(\sigma_{\Delta t}),$$

The function G_m describes the resolution of the detector for the measurement of Δt, which is assumed to be described by a single Gaussian distribution of width $\sigma_{\Delta t}$. Thus the CP violating rate asymmetry is represented by a constant term $\sin 2\phi$ that is modulated by a sine function of period $T = 2\pi/x$ and convoluted with the resolution function, G_m. The attenuation of the amplitude $\sin 2\phi$ remains small as long as $\sigma_{\Delta t} \ll T$. This observation has been verified by analytical calculations [34] and Monte Carlo simulations [35]. Figure 10 shows that the error in the CP term $\sin 2\phi$ depends only weakly on the uncertainty $\sigma_{\Delta t}$, which is related to $\sigma_{\Delta z}$, the error on the decay distance $\Delta z = z_{CP} - z_{tag}$ by:

$$\sigma_{\Delta t} \simeq \sigma_{\Delta z}/\beta\gamma c\tau.$$

The distances between the decay points of the two

Table 6: Estimated branching ratios and CP asymmetries for self-tagging decays, involving five quark level processes with penguin amplitudes.

Quark Process	Hadronic Decays	Branching Ratio	Rate Asymmetry
$b \to s\bar{c}c$	$B^- \to D^0 D_s^-$	$\sim 10^{-3}$	$\sim 0.5\lambda^4\eta \geq 2 \times 10^{-4}$
$b \to s\bar{u}u$	$B^+ \to K^+\pi^0$		
	$B^+ \to K^{*+}\pi^0$		
	$B^0 \to K^+\pi^-$		
	$B^0 \to K^{*+}\pi^-$	$\sim 10^{-5}$	$\sim 0.5\eta \simeq (5 \pm 3) \times 10^{-2}$
$b \to s\bar{s}s$	$B^+ \to K^+\phi^0$	$\sim 10^{-5}$	$\sim 0.5\lambda^2\eta \simeq 2 \times 10^{-3}$
	$B^+ \to K^{*+}\phi^0$	$\sim 3 \times 10^{-5}$	$\sim 0.5\lambda^2\eta \simeq 2 \times 10^{-3}$
$b \to d\bar{s}s$	$B^+ \to K^+\overline{K^0}$	$\sim 10^{-6}$	$\sim 0.5\eta \simeq (5 \pm 3) \times 10^{-2}$
$b \to d\bar{u}u$	$B^+ \to \pi^+\pi^0$	$\sim 10^{-5}$	$\sim 0.5\lambda^2\eta \simeq 2 \times 10^{-3}$

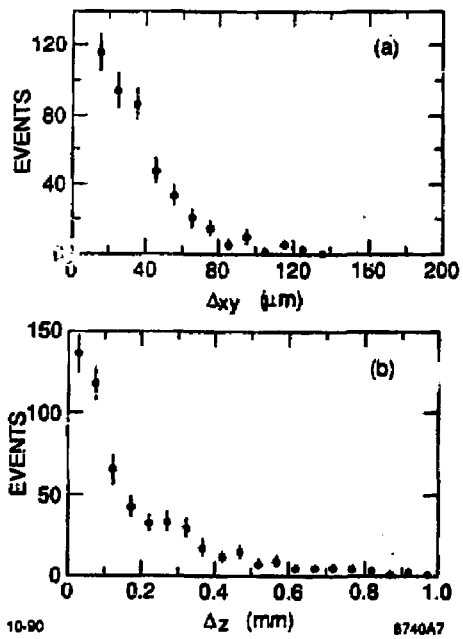

Figure 11: Distance between the decay points of the two B mesons (a) in the plane transverse to the beam and (b) along the direction of the beam, for beam energies of 9.0 on 3.1 GeV.

B mesons are shown in Figure 11, the averages are $\langle \Delta z \rangle = 180$ μm in the direction along the beam, and $\langle \Delta xy \rangle = 32$ μm in the plane transverse to the beam. Thus $\sigma_{\Delta z} < 0.5\beta\gamma c\tau$ translates to $\sigma_{\Delta z} < 90$ μm and—compared to a detector with perfect resolution—causes a dilution of the measurement of the CP asymmetry in B^0 decays by less than 10%.

B. Methods of Tagging the B^0 Flavour

At an $\Upsilon(4S)$ B Factory, the prepared initial state leads to an evolution of the B and $\overline{B}$ which is coherent, including the effects of flavour oscillations for neutral B mesons. Thus a constant phase relation is maintained, so that the two states remain orthogonal until one of them decays. If this decay at the time t_1 is flavour specific, it determines whether the other B decaying into a CP eigenstate at the time t_2 was a B^0 or $\overline{B}^0$ at the time t_1. The flavour of a B^0 can be derived from the presence of either a lepton from a semi-leptonic decay or a charged K from the secondary decay of a D meson. In both cases the charge of the particle tags the B flavour, i.e. e^+, μ^+, and K^+ tag a B^0 and e^-, μ^-, and K^- tag a $\overline{B}^0$. Two quantities characterize the tagging quality, the *tagging efficiency* ϵ, which is defined as the fraction of B^0 that are tagged, and w, the fraction of all tagged events that are incorrectly tagged.

Monte Carlo studies have been performed to develop efficient selection criteria for flavour tagging of decays to CP eigenstates [36]. Tagging leptons are required to have a momentum exceeding 1.4 GeV/c and a clean signal in the e.m. calorimeter or the muon detector. The efficiency for detecting one such lepton in

Table 7: The B^0 tagging efficiency ϵ and mistagging probability w based on a detector with a fully efficient Cerenkov counter and a dE/dx measurement with 7% resolution.

Tagging Method	ϵ	w
$\ell^{\pm}$	0.118	0.044
$K^{\pm}$ excl.	0.278	0.104
$K^{\pm}K^{\pm}$ excl.	0.011	0.051
Sum	0.407	0.088

Table 8: Resolution for vertex reconstruction based on a tracking system consisting of a 3 layer silicon strip vertex detector and a 39 layer central drift chamber with 10 μm and 150 μm resolution, respectively.

Decay Vertex	Resolution $\sigma_z(\mu m)$
$J/\psi K^0_S$	24
$\pi^+\pi^-$	27
D^+D^-	38 - 55
$\ell^{\pm}$ or $K^{\pm}$ tag	58

an event is $\epsilon = 11.8\%$, the probability for incorrectly tagged events is $w = 4.4\%$.

The flavour of the B^0 can also be tagged by the detection of 1 charged kaon or 2 like-sign charged kaons in the event. Assuming that the detector will be equipped with a fully efficient Cerenkov counter and a dE/dx system with a resolution of 7.5%, the kaon tagging efficiency is of the order of 33%, and 10% of the tags are incorrect. These estimates include the effect of kaon decay in flight.

The results for a combined tagging system are listed in Table 7. Here the lepton tag is assumed to take precedence over a kaon tag because of its smaller mistagging rate.

C. Vertex Reconstruction

The decay point of a B^0 to a CP eigenstate is determined from the reconstructed vertex of the prompt decay particles. Thus, for the $J/\psi K^0_S$ decay one uses the vertex of the reconstructed $J/\psi \to \ell^+\ell^-$ decay, while for the D^+D^- decays the B vertex is obtained from a fit of the two D decays projected back to their respective vertices. The uncertainty in the reconstruction of the vertices of various decays to CP eigenstates has been estimated by Monte Carlo simulations [37]. The results are listed in Table 8. The best resolution is obtained for the $J/\psi K^0_S$ decay mode, the resolution for the $D^{\pm}$ vertices depends critically on the number of π^0 in the decay.

The tagging vertex is reconstructed by fitting all charged particles that do not originate from the decay of the CP eigenstate to a common vertex, independent of the tagging method. Tracks from the decay of long-lived particles, such as K^0_S, Λ^0, or $\overline{\Lambda}$, are rejected by requiring that the impact parameter be less than 800 μm. No attempt has been made so far to separate D-meson tracks from prompt tracks. It is estimated that their effect on the measurement is not dominant, and to some degree cancels in the measurement of Δz, the distance between the two reconstructed decay points. The uncertainty of the reconstructed z position of the tag vertex is estimated to be 58 μm.

For many decay modes the error in the measurement of Δz is dominated by the error on the tagging vertex. For the CP eigenstate $J/\psi K^0_S$, it has been estimated by Monte Carlo simulation to be roughly $\sigma_{\Delta z} = 62$ μm. These results are fully compatible with the resolution necessary for the measurement of the CP asymmetry.

V. DETECTOR DESIGN

A. General Layout and Specifications

The design of a detector for an asymmetric $\Upsilon(4S)$ collider can be based on accumulated experience with detectors presently operating at the e^+e^- storage rings PEP, LEP, and particularly DORIS and CESR. Three novel features are needed: (a) solid angle coverage in the forward direction, (b) the detection of separate vertices along the beam direction, and (c) lepton detection and hadron identification up to 4.5 GeV/c momentum. A sketch of a detector lay-out is given in Figure 12. This lay-out was composed at the B-Factory Workshop at SLAC, and many of the parameters were derived from the CLEO II detector now operating at CESR.

To obtain high efficiency for complete event reconstruction, it is essential to cover as much of the solid angle as is practical. In Figure 13 the relation between the polar angle in the centre-of-mass and the laboratory system is illustrated.

In an asymmetric storage ring with beam energies of 3.1 GeV and 9.0 GeV, the $\Upsilon(4S)$ resonance is boosted

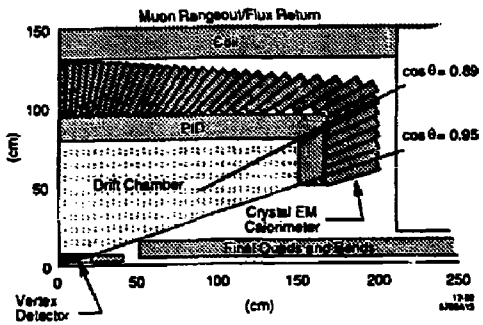

Figure 12: Lay-out of a detector for an asymmetric collider operating at the $\Upsilon(4S)$.

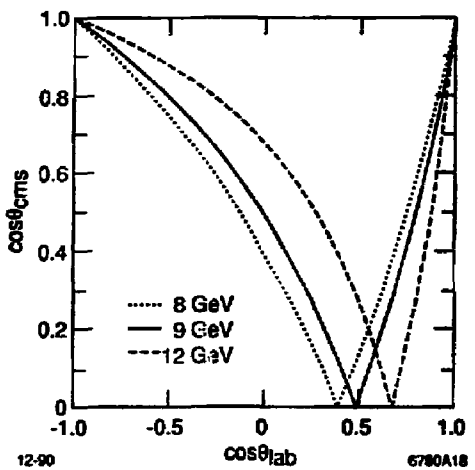

Figure 13: The detector coverage in the centre-of mass and the laboratory system for relativistic particles as a function of the energy of the high energy beam of an asymmetric B Factory.

with $\beta\gamma = 0.56$ along the direction of the higher energy beam. A coverage of $|\cos\theta_{cm}| = 0.91$ in the rest frame of the $\Upsilon(4S)$ corresponds to a polar angle coverage in the laboratory frame from $\cos\theta = -0.75$ to $\cos\theta = +0.97$. With this asymmetry in the beam energies, it is advantageous to place the detector such that the forward angle coverage is substantially larger in the direction of the higher energy beam.

The average charged particle multiplicity in the decay of the Υ resonance is less than 12, and apart from the effect of the relatively small boost along the beam direction, the particles are distributed rather uniformly. Such events do not require a detector with extremely good two-track separation and granularity.

B. Charged Particle Tracking

A typical charged particle tracking system consists of several components: a central drift chamber, a silicon vertex detector, and possibly an intermediate wire chamber. For this study, the central drift chamber (CDC) extends from 20 cm to 80 cm in radius, and it has 39 layers of sense wires placed at angles 0° and ±4° relative to the beam. The position resolution is taken to be 150 μm. The silicon vertex detector (SVD) is assumed to have 3 layers, at radii of 23,46, and 69 mm, and 10 μm resolution in both the xy and z direction. The vertex drift chamber (VDC), with 10 layers of alternating stereo angles of ±45°, has a position resolution of 50 μm. The CDC is filled with a gas of 450m radiation length, the VDC has a denser gas of 120m radiation length. The outer (inner) wall of the VDC is assumed to have a thickness of 2% (0.3%) of a radiation length. All other detector walls are less than $0.3\% X_0$.

For this combination of tracking devices, the resolution in the track parameters $\alpha_i = (1/p, b_{xy}, b_z, \phi, \theta)$, for momentum p, impact parameters b_{xy} and b_z, and angles ϕ and θ, has been studied for individual charged particles. The results are presented in Table 9 and Figure 14 [38]. They have been obtained from a fit to the track parameters, taking into account multiple scattering and intrinsic position errors and assuming cylindrical geometry. A solenoidal magnetic field of 10 kG is assumed. The error on a given track parameter α is usually expressed as a sum of two terms that are to be added in quadrature:

$$\Delta\alpha = A_\alpha \oplus C_\alpha/p[GeV/c].$$

The first term A_α describes the geometric resolution and is a function of most of the following parameters: the intrinsic resolution per layer, the number of layers, the stereo angle of the layers, the total length

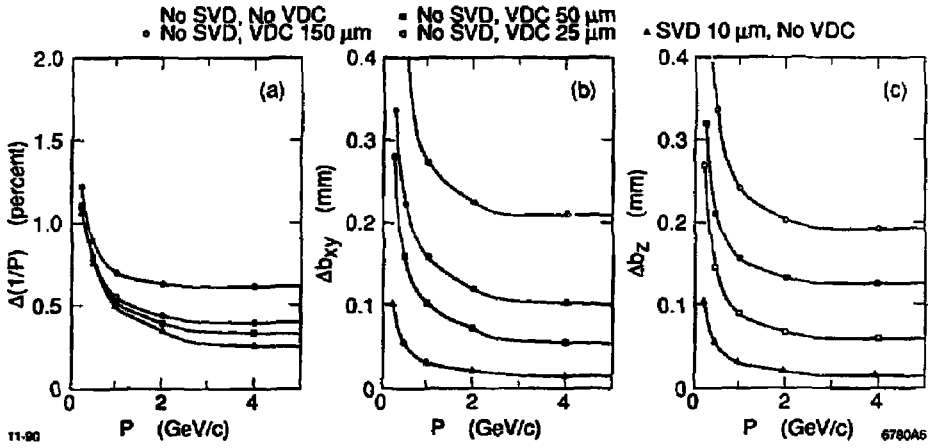

Figure 14: Resolution in track momentum and impact parameters for charged particles measured in either the CDC alone, the CDC and VDC, or the CDC and the SVD.

of the tracking device, and the polar angle of the track. In particular, $A_{1/p} \sim L^{-2}$, where L is the track length. The second term represents the contribution from multiple scattering, and is dominated by the amount of material in the beam pipe and the detector walls. It depends critically on the polar angle, i.e. $C_\alpha \sim \sin^{-n/2}\theta$, where n=5 for C_z (impact parameter b_z), n=3 for C_{xy} (impact parameter b_{xy}) and C_ϕ (azimuth angle ϕ), and n=1 for C_θ (polar angle θ). Table 9 lists the parameters A_α for combinations of different tracking devices. The last row gives the multiple scattering terms C_α for the CDC combined with the SVD. Most of the tracks emitted at small angles to the beam undergo larger multiple scattering and do not contribute to the determination of the vertex. They may, however, in many events aid in the reconstruction of exclusive decay modes.

Measurements of the track momentum p and angle ϕ rely primarily on the CDC. The addition of the VDC with 50 μm resolution improves the momentum resolution $\Delta p/p^2$ from 0.6% to 0.3%, where half of this improvement is due to the extension of the track length from 60 cm to 70 cm. The insertion of the silicon vertex detector further improves the momentum resolution to 0.2%, partly from the extension of the measured track length to 76 cm. The angular resolution is dominated by multiple scattering, and is about 1.2 mrad/p[GeV/c]. The most dramatic improvement achieved by the addition of the vertex detectors is the resolution in the polar angle θ and the impact parameter b_z. This is due to the much larger stereo angles of these devices.

In this study it was assumed that the VDC has 10 layers of signal wires of alternating +45° and −45° stereo angle. Such a chamber with a very unconventional wire suspension technique was built and installed by the ARGUS group at DESY. A position resolution of better than 40 μm was achieved over half the drift cell of 5.3 mm width [39]. For a track measured only in the VDC with stereo layers of alternating angle $\pm\mu$, the error in the impact parameter varies as $\Delta b_z = 86\ \mu\text{m}/\sin\mu$ and the polar angle error is $\Delta\theta = 0.7\ \text{mrad}/\sin\mu$. Thus a relatively large stereo angle, i.e. $|\mu| \geq 0.2$ mrad, would improve the matching of track elements in the CDC and the SVD. Figure 15 shows the resolution in impact parameter b_z and polar angle θ for different sequences of stereo layers with angles $\pm\mu$ in the VDC.

C. Silicon Vertex Detector

A finely segmented silicon vertex detector can provide a high precision measurement of the impact parameter, b_z parallel and b_{xy} transverse to the direction of the beam, and the angles, the azimuth ϕ and the polar angle θ, of charged particle tracks close to the beam-beam interaction point, and can thereby complement the angle and momentum measurement in the central tracking chamber.

Table 9: Charged particle track resolution for combinations of different devices: the CDC (Central Drift Chamber), the VDC (Vertex Drift Chamber), and the SVD (Silicon Vertex Detector). The last line lists the contributions from multiple scattering for a track of 1 GeV/c and $\cos\theta = 0$.

Device	Measurement	Stereo Angles	Radial Length	$A_{1/p}$ [%]	A_ϕ [mrad]	A_{z_0} [μm]	A_θ [mrad]	A_z [μm]
CDC	39 ×150 μm	0°, ±4°	60 cm	0.60	0.91	206	3.52	1744
CDC	39 ×150 μm	0°, ±4°						
VDC	10 × 50 μm	±45°	70 cm	0.31	0.36	46	0.99	124
CDC	39 ×150 μm	0°, ±4°						
VDC	10 × 50 μm	±45°						
SVD	6 × 10 μm	0°, 90°	76 cm	0.16	0.18	10	0.24	13
CDC	39 ×150 μm	0°, ±4°						
SVD	6 × 10 μm	0°, 90°	76 cm	0.20	0.20	11	0.30	15
m.sc.			76 cm	0.46	1.21	29	1.20	28

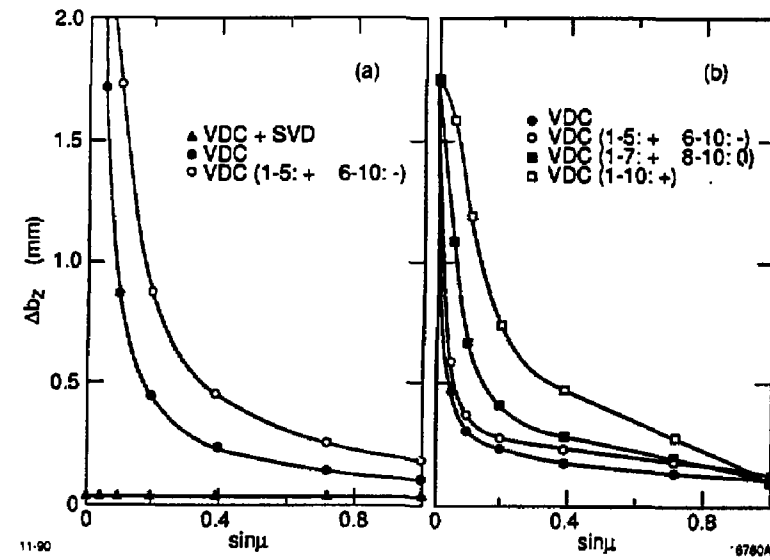

Figure 15: Resolution in the impact parameter b_x for tracks of 1 GeV/c momentum and cos θ=0 as a function of the stereo angle μ of the wires in the VDC, (a) for the VDC measurement alone, and (b) for a combined tracking system including the CDC. The different curves refer to different sequences of stereo angles ($\pm\mu$) in the 10 layers.

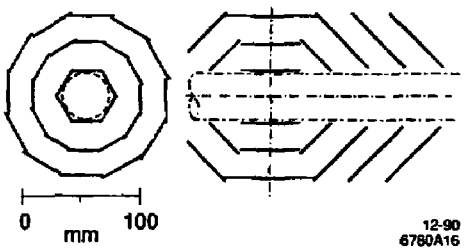

Figure 16: Schematic lay-out of a silicon strip vertex detector.

At a high luminosity B Factory, the primary task of the vertex detector will be the measurement of distance between the two B^0 decay points permitting the measurement of time dependent CP asymmetries. It will also help to reduce the background for leptons and kaons that determine the flavour of the second B^0 or $\overline{B}^0$ in the event. In addition, good vertex resolution will be important for many other measurements. For example, charm, beauty and $\tau^+\tau^-$ events can be separated through vertex topology from light quark processes, thus reducing combinatorial background in mass distributions.

The requirement that the B decay vertex be well measured in the direction along the beam demands silicon detectors with a coordinate read-out transverse to the direction of the beam. This is different from all present applications of such devices at colliding beam machines. While vertex detection along the beam axis is mandatory, a good measurement would still be desirable in the x-y plane. Thus silicon detectors with read-out in two orthogonal coordinates are necessary. This can be done either using pairs of single-sided or double-sided strip detectors or pixel arrays with direct read-out.

Lay-out

A schematic lay-out of a silicon strip vertex detector is given in Figure 16. It is cylindrically symmetric relative to the beam. The detector modules are arranged such that any particle emitted from the beam centre will traverse three planes, each measuring two orthogonal coordinates. In the central section the modules are of rectangular shape, while the endcap detectors are arranged to form twelve-sided pyramids with a trapezoidal shape. For a typical strip pitch of 50 μm and a strip length of 2-4 cm the segmentation is 50-100 strips/cm^2. There is a total of 74k strips in the central, and 86k strips in the endcap section. The segmentation requirements are not set by the multiplicity of the decay particles, but by the additional signals generated by beam related background. The choice is also influenced by the maximum input capacitance per channel which is compatible with the design of low noise and low power amplifier circuits.

Track reconstruction errors have been studied for silicon detector as a function of detector spacing, detector and beam pipe thickness, intrinsic resolution, etc. [40]. The results were obtained from a fit to the track parameters, taking into account multiple scattering and intrinsic position errors. The detectors are equally spaced in radius, $r_1 = 23$ mm, $r_2 = 46$ mm, $r_3 = 69$ mm. They are assumed to be 300 μm thick, and to have a constant position resolution of 10 μm in the two orthogonal coordinates $d_i = r_i\phi$ and $z_i = r_i \cot\theta$.

This study ignores the degradation of the position resolution for non-normal incidence [41]. The calculations assume cylindrical detector planes of unlimited length. In a realistic design, endcap detectors would be introduced to reduce the effects of multiple scattering and the problems of non-normal incidence. Also not included are errors in the placement and alignment of the detector modules, instabilities in their position with time and possible effects of temperature changes during operation.

Intrinsic resolution

The resolution in the impact parameter and angles is expected to depend linearly on the single point measurement error. However, as we see in Figure 17a, for particles with less than 1 GeV/c momentum, multiple scattering dominates. For perpendicular incidence, the difference between a detector of 10 μm resolution and a perfect detector corresponds a change in the impact parameter error from 25 μm to 31 μm.

Beam pipe radius

Figure 17b shows the resolution as a function of the radius of the inner layer r_1 (the inner beam pipe radius is taken to be 3 mm smaller than r_1) for a fixed spacing of the two layers of $\Delta r = 46$ mm. It is obvious that the impact parameter measurement is most sensitive to the radius of the innermost layer and the beam pipe inside. A reduction of the inner radius by 10 mm would improve the impact parameter resolution from 30 μm to 18 μm.

Beam Pipe and Detector Thickness

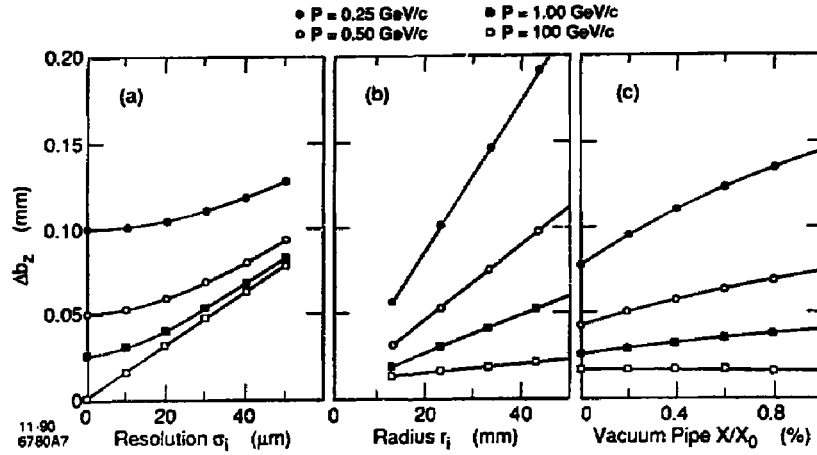

Figure 17: Resolution in the impact parameter b_z as a function of (a) the intrinsic detector resolution σ_i, (b) the radius of the first layer outside the beam pipe, and (c) the thickness of the beam pipe for tracks of different momentum measured in the x-y plane.

We have chosen to place the detector outside of the vacuum chamber because this will avoid problems of assembly, access, vacuum feedthroughs, etc. and will not substantially increase the amount of multiple scattering so critical here. We have assumed a double walled pipe made of 2 × 0.5 mm of beryllium (0.28%X_o). This will allow for a cool gas to be pumped in the annulus between the two walls to carry the heat load from the beam. A liquid coolant would increase the thickness by typically 0.14%X_o. Such a pipe will also have the skin depth needed to shield the detectors and their electronics from the beam. In practice, a lining of a few μm of copper is added on the inside, to absorb soft photons from synchrotron radiation. Figure 17c shows the effect of variable beam pipe thickness on the error in the impact parameter b_z. Over this limited range the resolution varies roughly linearly with the beampipe thickness, from a minimum of 25 μm for zero thickness to 40 μm for a beampipe of 1.0% of a radiation length. Doubling the detector thickness from 300 to 600 μm increases the resolution from 31 to 36 μm at normal incidence, and from 93 to 115 μm at $\cos\theta = 0.8$.

Number of Layers

In principle, one only needs two planes to measure positions and angles. In practice, there are inefficiencies due to dead channels, edges, and possibly support structures so that the addition of a third layer reduces detection losses. Pattern recognition in the presence of background requires at least one redundant measurement, and benefits greatly from additional measurements. Additional layers do not improve the resolution, but they do not seem to hurt, even at very low momentum. However, effects of energy loss, interactions or absorption, delta rays, etc. have not been studied. Except for the highest momenta, the impact parameter error and angular resolution are not very sensitive to the layer spacing.

Conclusions

Based on the present lay-out of the IR region with a vacuum pipe made of 1 mm of beryllium and a radius of 20 mm, a silicon vertex detector can measure impact parameters of charged particles of 1 GeV/c momentum to an accuracy of 50 μm or better over a large fraction of the solid angle. The angular resolution is of the order of 2 mrad or better in azimuth and polar angle. This can be achieved with double-sided strip read-out or pixel devices of 50 μm strip pitch or pixel size. The development of low power, low noise, high density amplifiers and read-out circuits needs to be pursued so as to fit the detectors into the limited space without loss of solid angle cov-

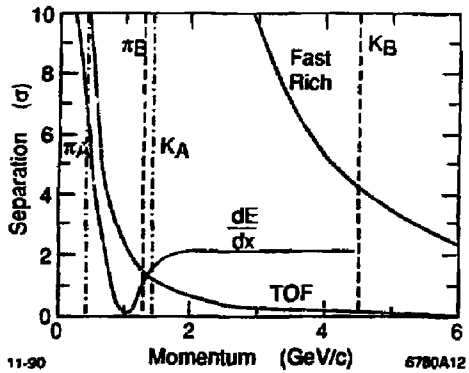

Figure 18: Predicted π/K separation as a function of the particle momentum for different devices: (a) TOF system at 1.1m with a resolution of 150 ps folded in quadrature with a 50 ps uncertainty due to the bunch length; (b) dE/dx for 60 x 1 cm samples in a drift chamber filled with a He based gas mixture; refraction of n=1.006 and 1.06.

erage, and without a substantial increase in multiple scattering. Techniques for cooling, precision assembly and alignment need to be developed.

D. Particle Identification

The separation of pions from kaons is essential both for the selection of exclusive B and D decays and for the determination of the flavour of the second B meson in the event by the identification of a kaon of specific charge. $K^{\pm}$ mesons from B decays have an average momentum of 0.85 GeV/c, and 30% of all kaons have momenta above 1 GeV/c. Exclusive two-body decays, like $B^0 \to K^+\pi^-$, pose the biggest challenge to the particle identification system, because their momentum spectra extend from 1.5 to 4.5 GeV/c. Their angular distribution is strongly peaked due to the asymmetry in the beam energies.

There are three basic techniques that represent more or less viable options for particle identification at a B Factory: precision time-of-flight (TOF), dE/dx measurements in the tracking chamber, and Cerenkov counters. The predicted π/K separation as a function of momentum is shown in Figure 18 for these different devices.

Time-of-Flight Measurement

The TOF technique using scintillation counters is simple and well understood at low momentum, but above about 1.0 GeV/c it requires either unprecedented precision or flight paths that are unacceptably large.

dE/dx Measurement in the CDC

Modest quality dE/dx in a central tracking chamber can provide good hadron separation in the $1/\beta^2$ region and help in low momentum e/π discrimination. It is likely to be employed in any tracking device, because it is essentially "free." However, above 1.5 GeV/c one operates in the region of the relativistic rise of the energy loss, and many samples (and therefore a large chamber) are needed. This also calls for a heavier gas (perhaps pressurized) than would be desirable for the best tracking resolution. In addition, the existence of a "cross-over" between the $1/\beta^2$ and relativistic rise regions requires that any dE/dx system must be combined with another technology if complete momentum coverage is to be attained. In such a combined system the central tracking chamber performs "double duty", resulting in simple and uniform track matching down to small polar angles.

Fast Ring Imaging Cerenkov Counters

The third (and leading) contenders for hadron identification at the B Factory are Cerenkov counters. Threshold or ring imaging techniques could provide adequate performance, provided that the efficiency for Cerenkov photon detection is sufficiently high. The primary advantages over dE/dx are that these devices (a) have excellent hadron separation over the full momentum range at a B Factory, and (b) are fully modular and separable from the tracking, allowing the optimization of the tracking independent of particle ID concerns. Conversely, these Cerenkov devices are more challenging to construct and operate, are more difficult to build in a fully hermetic configuration, and add substantial amounts of material in front of the e.m. calorimeter.

One very attractive solution to the problems posed by the standard CRID design is the so-called "Fast" RICH. In this device the three-dimensional TPC readout is replaced by a photocathode with a short absorption length and a two-dimensional pad read-out. Since the photo-electron produced by the Cerenkov light has a short drift length, the drift time is also short and the device is fast.

A reflective CsI photocathode with an absorbed film of TMAE is combined with a liquid C_5F_{12} radiator. This novel cathode has a superior quantum ef-

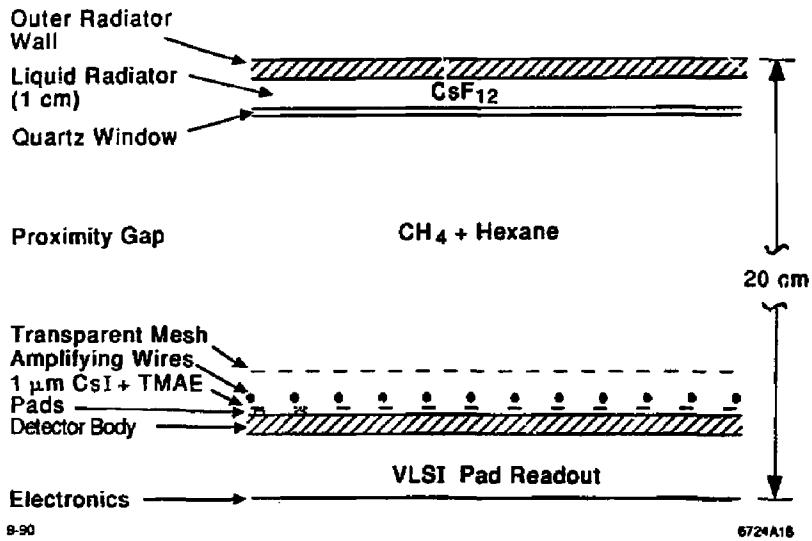

Figure 19: Schematic cross section for a liquid radiator RICH with a reflected proximity gap and a *CsI* cathode coated with TMAE.

ficiency over the entire wavelength region of interest. It is well adapted to fast RICH counters because of its isochronous signals and room temperature operation. The *CsI* cathode operates in the 6-7 eV photon region where fluoro-carbon liquids and quartz windows transmit well, so that expensive, dispersive solids, like *NaF*, are not needed for radiators or windows. Hexane gas is added to the methane chamber atmosphere to eliminate the UV feedback photons above 7.0 eV. A VLSI pad readout is under development.

For particles of normal incidence the amount of material in this device is estimated to be about $12 - 15\% X_o$. The portion contributed by the material farthest from the calorimeter, i.e. the detector and readout chips, is only about 2.5% X_o.

Aerogel Threshold Cerenkov Counters

In comparison with RICH counters, threshold Cerenkovs are rather simple devices. Figure 20 shows the schematics of a double cell detector element. These thin-walled cells are filled with aerogel of different density and index of refraction, resulting in different thresholds for the Cerenkov radiation, namely $n_1 = 1.006(\beta > 0.994)$ and $n_2 = 1.06(\beta > 0.943)$. The total thickness is less than $5\% X_o$. The optical and mechanical properties of silica aerogels are directly linked to their micro-structure consisting of colloidal connected spheres of SiO_2 (4 - 6 nm in diameter) with pores of variable size. Densities can be varied in the range 3-600 mg/cm^3, corresponding to indices of refraction between 1.0006 and 1.126. Silica aerogel of low density is a sponge-like, very fragile substance that exhibits Rayleigh scattering, primarily in the blue region of the visible spectrum (it looks like "frozen smoke"). This, combined with high transmission in the visible and infrared region, results in non-directional light output from Cerenkov radiation. Aerogels can be doped with wavelength shifters to match the photon spectrum to the sensitivity of the photo-triode or single photon avalanche diode read-out [44]. The use of aerogel was first suggested by E. Lorenz [42]. Studies of its optical properties have just begun, and various ideas for the read-out and the design and fabrication of a large hermetic system are being explored [45].

E. Electromagnetic Calorimeters

An electromagnetic calorimeter with good photon resolution from 10 MeV to 4 GeV and large solid angle coverage will greatly enhance the reconstruction of B decays involving π^0 or J/ψ mesons, as well as the detection of electrons from semi-leptonic B decays,

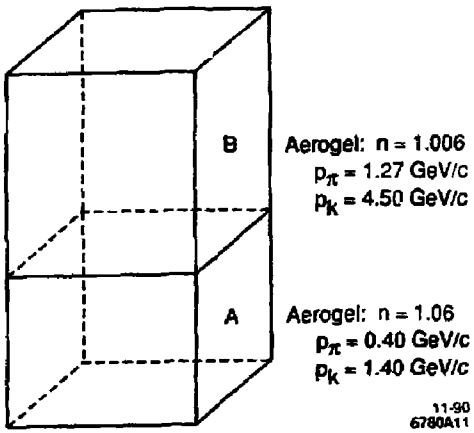

Figure 20: Schematics of a two-cell aerogel Cerenkov counter.

and photons from radiative decays or transitions to χ_b states. The goal is to achieve an energy resolution of

$$\frac{\sigma_E}{E} = \frac{2\%}{\sqrt[4]{E(GeV)}} \oplus 1\%$$

and an angular resolution of 5-10 mrad. These specifications narrow the choices to two techniques, either a liquid krypton calorimeter or a hermetic array of CsI crystals.

Liquid Krypton Calorimeters

A krypton filled, total absorption calorimeter with pad read-out arranged in projective towers of constant solid angle was studied during the B-Factory Workshop at SLAC [46]. A prototype detector was built and tested at Novosibirsk for use in the KEDR detector at the VEPP-5 storage ring [47]. Because of the slow drift velocity of ions in krypton, the signal is derived by integration over 1/10 of the total drift time of $6\mu s$. Also, an analog energy sum will suffer from coherent noise in the detector. A calorimeter based on a liquid radiator offers advantages in the ease of calibration, radiation hardness, and cost (which is completely dominated by the availability and cost of the krypton). The major disadvantage is the longer radiation length, the slow charge collection and poor time resolution ($\lesssim 600ns$), the limited hermiticity and the total thickness of the cryostat walls. For a device with an inner radius of 1 m, the total thickness of the cryostat walls adds up to 20%-30% of a radiation length.

CsI Calorimeters

A crystal calorimeter segmented into roughly 10,000 elements is the premier choice for a B Factory. It meets the specifications, has excellent time resolution to allow for fast triggering, and permits a high degree of hermiticity. Its disadvantages are sensitivity to radiation damage, need for constant calibration and monitoring, and relatively high cost. A large calorimeter made of thallium doped CsI has been built and installed in the CLEO II detector at CLEO. First results are now available and show impressive performance [49]. $CsI(Tl)$ was chosen because of its large photon yield, cost and availability in industry. BGO is more expensive given an inner radius of 1m, BaF_2 has recently become available in form of 25 cm long crystals [50]. $NaI(Tl)$ is more fragile and more hygroscopic, and has a longer radiation length.

Several read-out methods have been discussed. The CLEO group has chosen 4 silicon photodiodes with charge sensitive amplifiers per crystal. This adds electronic noise at the level of 0.6 MeV per crystal and limits the resolution at low energy. As an alternative, a two-stage photomultiplier could be used as an essentially noiseless amplifier. Such a device can operate in a magnetic field, provided its axis is within 45° of the field axis.

The radiation resistance of the crystal material is of concern, primarily for the endcap section. Pure CsI is known to be less susceptible to radiation damage than $CsI(Tl)$, but it produces a factor of five less light. Therefore, a thick tungsten shield surrounding the beam outside the central IR is foreseen to protect against large beam losses during injection and machine studies.

As an illustration of the performance of a $CsI(Tl)$ calorimeter, Figure 21 shows data from the CLEO II detector. A clear signal for π^0 and η^0 is observed. The rms width of the π^0 mass peak varies between 5 MeV at low momentum to 9 MeV above 3 GeV where the two showers begin to merge. The gain has been calibrated using Bhabha scattering, and a resolution of 1.3% at 5 GeV obtained.

Material in Front of the Calorimeter

A major consideration for the choice of the most suitable e.m. calorimeter is the amount of material in front, including the particle identification system. A Monte Carlo study was performed [48] to estimate the energy loss and the degradation in the photon energy resolution as a function of the photon energy and angle of incidence. The results are presented in Ta-

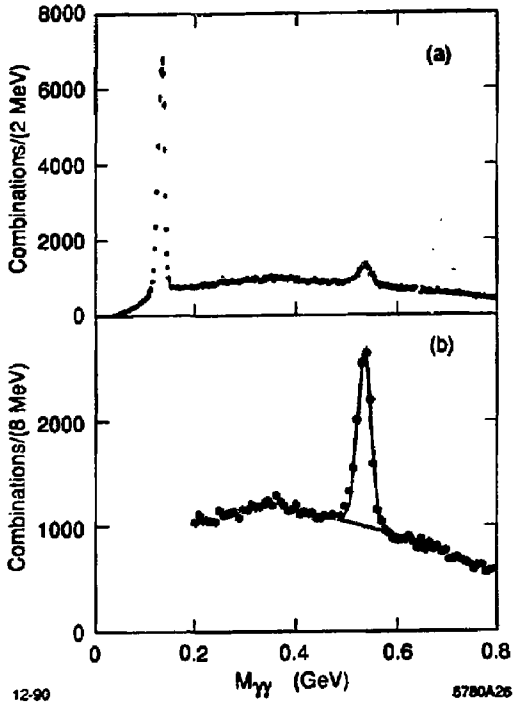

Figure 21: $\gamma\gamma$ mass spectra measured in the CLEO II *CsI(Tl)* detector.

Table 10: Mean and (in parentheses) rms of the energy loss (in MeV) for 10 MeV and 100 MeV photons, as a function of the polar angle θ and the thickness d of the material in front of the calorimeter (in units of X_o).

d	E_γ = 10 MeV		E_γ = 100 MeV	
	$\theta = 90°$	$\theta = 35°$	$\theta = 90°$	$\theta = 35°$
0%	0.02 (0.36)		0.10 (0.65)	
5%	0.1 (0.5)	0.2 (0.9)	0.2 (1.1)	0.4 (1.7)
10%	0.2 (1.1)	0.5 (1.9)	0.4 (1.9)	1.1 (3.6)
20%	0.6 (2.1)	1.2 (3.0)	1.2 (3.6)	3.7 (8.7)
40%	1.3 (3.1)	2.5 (4.0)	4.0 (9.1)	12. (20.)

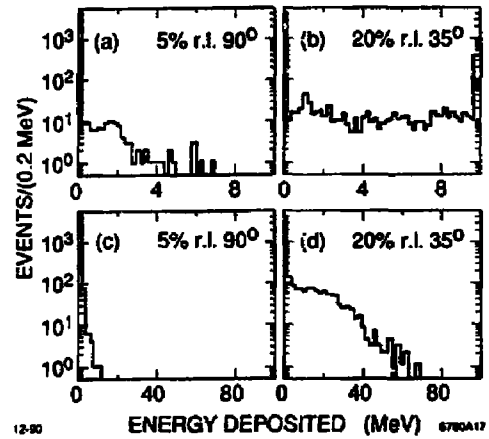

Figure 22: Energy deposition of photons of (a-b) 10 MeV and (c-d) 100 MeV at angles of 0° and 35°.

ble 10 and Figure 22. The energy loss distribution is very non-gaussian, and its rms is comparable to the mean energy resolution targeted for the calorimeter. It is conceivable that an interaction in the material in front of the calorimeter could be detected. However, it is unlikely that the deposited energy could be measured with sufficient precision to allow for an adequate correction. Thus, to achieve the resolution stated above it is necessary to keep the amount of material in front of the calorimeter to less than 10%-15%X_o. This not only excludes the use of a cryogenic calorimeter, but also disfavours the RICH for particle identification. It also demands that the drift chamber endplates be very thin so as not to seriously affect the resolution in the calorimeter endcaps.

F. Muon Detector

The detection of $\mu^\pm$ with momenta as low as 0.5 GeV/c greatly enhances the efficiency for flavour tagging and J/ψ reconstruction. Below 1.2 GeV/c the difference in range between pions and muons permits a good separation, and a detector composed of thin tracking chambers sandwiched between iron absorber plates of less than 1 cm thickness could surround the e.m. calorimeter. For higher momenta, thicker plates on the outside could be used to absorb strongly interacting pions and kaons. More detailed studies are needed to establish a credible $\mu^\pm$ detector design.

REFERENCES

[1] The following persons contributed to the activities of Session 2.3:

B-Factories: P.Avery (Florida), D.Britton (McGill), T.Browder (Cornell), F.Bulos (SLAC), D.Cassel (Cornell), D.Coupal (SLAC), N.G.Deshpande (Oregon), H.DeStaebler (SLAC), J.Dorfan (SLAC), D.Hitlin (Caltech), B.Kayser (NSF), K.Kinoshita (Harvard), F.Le Diberder (SLAC-Saclay), H.Lipkin (Weizmann), A.Lu (UCSB), N.Mistry (Cornell), B.Niczyporuk (CEBAF), P.Patel (McGill), J.Rosner (Chicago), H.D.Schulz (DESY), A. Snyder (SLAC), S.Stone (Cornell), W.Toki (SLAC), S.Wagner (SLAC), and M.Witherell (UCSB).

Φ Factories: C.Bloise (Frascati), P.Campana (Frascati), and D.Cline (UCLA).

τ/c Factories: Huishun Mao (IHEP Beijing), and Zhao-Xi Zhang (ITP Beijing).

[2] "Proposal for an Electron Positron Collider for Heavy Flavour Physics and Synchrotron Radiation", PSI report PR-88-09 (1988).

[3] "Feasibility Study for a B-Meson Factory in the CERN ISR Tunnel", ed. by T.Nakada, CERN report 90-02 (1990).

[4] *Proceedings of the Workshop Towards Establishing a b Factory*, ed. by M.Goldberg and S.Stone, Syracuse (1989); "Prospects for a CESR B-Factory Upgrade", CLEO preprint CLNS 89/962 (1989).

[5] *Proceedings of the Workshop on Detectors for an Asymmetric B Factory*, MPI report H-1990-V6, Heidelberg (1990).

[6] *Proceedings of the B Factory Workshop at KEK I and II*, October and March, 1989.

[7] "The Physics of a High-Luminosity Asymmetric B Factory at SLAC", ed. by D.Hitlin, SLAC report 353 (1989).

[8] *Proceedings of the Workshop on Physics and Detector Issues for a High-Luminosity Asymmetric B Factory*, ed. by D.Hitlin, in preparation.

[9] See discussions in references [1-7] for example.

[10] I.I.Bigi and A.I.Sanda, Nucl. Phys. **B193** (1981) 85; Nucl. Phys. **B281** (1987) 41; I.I.Bigi, V.A.Khoze, N.G.Uraltsev and A.I.Sanda in *CP Violation* (World Scientific Series on Directions in High Energy Physics, vol. 3). See also, I.Dunietz and J.L.Rosner, Phys. Rev **D34** (1986) 1404 and references therein.

[11] L.L.Chau and W.-Y.Keung, Phys. Rev. Lett. **53** (1984) 1802; J.D.Bjorken, Fermilab report, 1988 (unpublished).

[12] R.Fulton *et al.* (CLEO), Phys. Rev. Lett. **64** (1990) 16.

[13] H.Albrecht *et al.* (ARGUS), Phys. Lett. **234B** (1990) 409;
H.Albrecht *et al.* (ARGUS), "Reconstruction of Semileptonic $b \to u$ Decays", DESY preprint 90-121 (1990).

[14] C.O.Dib, I.Dunietz, F.J.Gilman, and Y.Nir, Phys.Rev. **D41** (1990) 1522.

[15] L.Wolfenstein, Phys.Rev.Lett. **51** (1983) 1945.

[16] G.J.Feldman *et al.*, Proceedings of the Summer Study on High Energy Physics in the 1990s, Snowmass (1988) p.561.

[17] P.Oddone, *Proceedings of the UCLA Workshop: Linear Collider $B\overline{B}$ Factory Conceptual Design*, ed. by D.Stork (1987) p.243.

[18] R.Aleksan, J.Bartelt, P.R.Burchat, and A.Seiden, Phys. Rev. **D39** (1989) 1283.

[19] For a more detailed discussion see F.Porter *et al.*, SLAC B-Factory Workshop, BaBar Note #26 (1990).

[20] D.Besson *et al.* (CLEO), Phys. Rev. Lett. **54** (1985) 381.

[21] G.J.Feldman *et al.*, *op cit.*; Modification to include signal-to-background contribution in F.Porter *et al.*, SLAC B-Factory Workshop, BaBar Note #31 (1990); N.Mistry and T.Browder, private communication.

[22] T.Browder, contribution to this workshop.

[23] B.Kayser, contribution to this workshop.

[24] H. J. Lipkin, preprint WIS-90/23/MAY-PH, Wisconsin (1990).

[25] W. Toki, SLAC B-Factory Workshop, BaBar Notes #43 (1990).

[26] I. Dunietz, H. Quinn, W. Toki, A. Snyder, and H.J. Lipkin, SLAC-PUB 5270 (1990), submitted to Physical Review.

[27] H. J. Lipkin and A. I. Sanda, Phys. Lett. **201B**, (1988) 541, and B. Kayser, M. Kuroda, R.D. Peccei, and A.I. Sanda, Phys. Lett. **237B** (1990) 508.

[28] H. Schröder, in *Proceeding of the Int. Conference on High Energy Physics*, Singapore (1990).

[29] W. Toki, SLAC B-Factory Workshop, BaBar Notes #52 and #53 (1990).

[30] R.Aleksan, I.Dunietz, B.Kayser and F.Le Diberder, "CP Violation using non-CP Eigenstate Decays of Neutral B Mesons", Saclay preprint DPhPE 90-17 (1990).

[31] J.-M. Gerard and Wei-Shu Hou, preprints PSI-PR 90-25 and PSI-PR 90-34.

[32] L. Wolfenstein, preprint NSF-ITP 90-29.

[33] N.G. Deshpande and J. Trampetic, Phys. Rev. **D41** 895 (1990), preprint OITS 420 (1990), and N.G. Deshpande preprint OITS 460 (1990).

[34] F. LeDiberder, SLAC B-Factory Workshop, Babar Note #34 (1990).

[35] F. LeDiberder, W. Toki, M. Witherell, SLAC B-Factory Workshop, Babar Note #45 (1990).

[36] S. Komamiya, SLAC B-Factory Workshop, BaBar Note #56, (1990).

[37] S. Komamiya, SLAC B-Factory Workshop, BaBar Note #56, (1990); S. Wagner and Art Snyder, contribution to this workshop; F. LeDiberder, contribution to this workshop; These results have recently been confirmed on the basis of Paul Avery's Monte Carlo simulations performed at Cornell.

[38] V. Lüth, contribution to this workshop.

[39] E. Michel et al., Nucl. Inst. Methods, **A283**, 554 (1989).

[40] V. Lüth, Design of a Silicon Vertex Detector, SLAC B-Factory Workshop, Babar Note #55 (1990).

[41] V. Lüth, Spatial Resolution of Silicon Detectors, SLAC B-Factory Workshop, BaBar Note #48, (1990).

[42] R. Arnold, et. al., Design Proposal for a B-Factory Detector at PSI (1988).

[43] J. Seguinot, Proceedings of the Symposium of Particle Identification at High Luminosity Hadron Coilliders, April 1989, Fermilab, Batavia, Ill.; T. Ypsilantis, Ibid.

[44] G. Eigen (CALTECH) and L. Hrubesh (LLL), private communication.

[45] G. Eigen, contribution to the SLAC B-Factory Workshop (1990).

[46] G. Godfrey, contribution to the SLAC B-Factory Workshop (1990).

[47] A. Chilingarov, private communication.

[48] H. Marsiske, contribution to the SLAC B-Factory Workshop (1990); F. Bulos, D. Hitlin, contribution to this workshop.

[49] T. Skwarnicki, in Proc. of the *Int. Conference on High Energy Physics*, Singapore (1990).

[50] S.C.C Ting in *Letter of Intent for a Detector for the SSC (1990)*. The crystals are available from the Changhai Institute of Ceramics, at a present cost of $\$3.50/cm^3$.